

A General Method for Determining Sample Efficiencies in Liquid Scintillation Counting

Willard G. Winn

ABSTRACT

Many modern liquid scintillation counters use two coincident photomultiplier (PM) tubes to reduce background noise. These counters detect most charged particle emitting nuclides with an efficiency near 1; however, they are noticeably less efficient for detecting lower energy emissions from nuclides such as tritium, because each decay produces so few photons that any coincident detection is less probable. For quenched samples, the photon production is further reduced, yielding a corresponding contraction of the observed energy spectra. The probability (or efficiency) for detecting a charged particle increases from 0 to 1 as its photon production (or its energy) increases from 0 to higher values. A model for this probability was developed and tested against experimental measurements.

A trinomial probability distribution modeled the efficiency as a function of observed spectral energy. The three probabilities of the trinomial include two for photon detection by the two PM tubes and one for nondetection. For a TRI-CARB 2000 CA/LL liquid scintillation analyzer, reasonable efficiency models resulted when using the trinomial formalism as a basis for empirically selecting the efficiencies. Using measurements of low-energy Auger and conversion electrons of quenched ^{57}Co standards as an experimental guide, four efficiency curves were modeled and tested. Scintillation spectra of ^3H and ^{14}C quenched standards were convoluted with the efficiency curves to test each model. The dpm predicted by the best model agreed with that known for the standards, provided that $\text{cpm/dpm} > 0.25$. The method may be extended down to $\text{cpm/dpm} \approx 0.1$ by incorporating a "bootstrap" correction technique.

INTRODUCTION

At the Savannah River Site (SRS), waste that is classified as nonradioactive hazardous liquid waste must be certified as having a total activity less than the DOT requirement of 2 nCi/g before it can be shipped off plant for disposal.¹ Reliable methods for determining the total activity of samples, therefore, have received much attention at SRS.

Liquid scintillation counting is capable of detecting all types of nuclear decays, making it an attractive waste appraiser. It is particularly suited for detecting nuclides that decay by α and β^\pm emission. Some nuclides decay by

electron capture (EC), but even these emit detectable Auger electrons and X-rays. Also, any accompanying γ -ray and conversion electron (ce) emissions may be detected. Unfortunately, the detection efficiency for the various decay modes can differ substantially, and many can have efficiencies well below 100%.

Over the years, various techniques have evolved for establishing liquid scintillation counting efficiencies. Examples of these include the channels ratio method,² efficiency tracing,³⁻⁵ extrapolation,⁶ internal/external quench standards,^{2,7,8} and direct modeling of the efficiencies per basic detection processes.⁹⁻¹⁴ These techniques have primarily been developed for β -emitters, but some can be extended to other types of radionuclide emissions. In particular, direct modeling promises to be useful for all emissions of interest. It assumes that the energy spectrum is known. This allows efficiency modeling based on the number of photons generated in the liquid scintillation cocktail and their fraction detected by the photomultiplier tubes. By contrast, in waste samples, a priori knowledge of the true energy spectrum cannot be assumed; the detected spectrum is distorted by an energy-dependent efficiency that results from the photon generation and detection probabilities. Nevertheless, the detected spectrum does include information for inferring the nature of the true spectrum and its detection efficiency.

The present work explores a method for using the detected energy spectrum to infer the efficiency for a given sample. The method is developed using a TRI-CARB 2000 CA/LL scintillation counter which incorporates two coincident PM tubes to reduce background noise. Such a design is very popular in modern scintillation counters; however, the probability for detecting a pair of coincident photons from a nuclear decay event varies from 0 to 1 depending on the total number of photons produced. Because the spectral energy corresponds to the number of coincident photons detected, each energy of a spectrum should correlate with a probability for detection. It is clear that this detection probability should be close to 0 for the lowest spectral energies and should approach 1 as the energy increases. The present study develops and tests models for this probability.

THEORY

Conceptual Approach

Each decay event detected within a liquid scintillation spectrum has a probability associated with its detection, and its energy response is proportional to the number of photons detected. The probability of coincident photon detection increases with the number of photons emitted per decay event; thus, the detection probability increases as the spectral energy increases, as shown in Figure 1. For a typical sample, the detected energies are distributed over a spectral range. The probability for the number detected at each energy must be

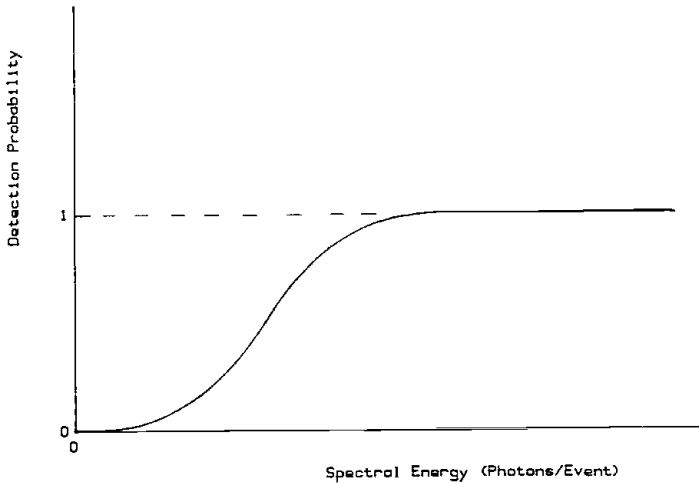


Figure 1. Figure 1. General trend of probability for detecting a pair of coincident photons produced by a nuclear decay event.

considered. Using these probabilities to perform an efficiency correction for counts collected at each point in the spectrum, the integral of these results should yield the total decays represented by the spectrum.

An example of the above concept is inherent in typical quench curves for ^3H and ^{14}C , as shown in Figure 2a.¹⁵ The spectra of quenched samples are contracted to lower energies. Their efficiencies are lower because fewer photons are produced per decay event. The plotted quench parameter tSIE is proportional to the energy range of spectra, calculated from the Compton spectrum of an external ^{133}Ba source.^{8,15} A tSIE of 1000 corresponds to the unquenched case. As the spectra are contracted to lower energies (more quenching), the attendant dropoff in efficiency is consistent with the type of detection probability illustrated in Figure 1.

Because all β -spectra have approximately the same shape when scaled to their maximum endpoint energies E_β , it is interesting to combine the ^3H and ^{14}C quench curves into a single plot, as shown in Figure 2b. In this plot, the efficiencies are plotted against $\text{tkeV} \equiv \text{tSIE}/1000 \times E_\beta$, where $E_\beta = 18.6 \text{ keV}$ for the ^3H data and $E_\beta = 156.5 \text{ keV}$ for ^{14}C . For tSIE = 1000, the defined tkeV corresponds to the true endpoint of the unquenched spectrum. For lower tSIE, the tkeV approximates the endpoints of the contracted β -spectra, which, in turn, approximate real unquenched spectra with these endpoint energies. The tkeV approximation yields a discrepancy between the ^3H and ^{14}C values in the overlap region at 15 to 20 keV; this is probably caused by resolution broadening of the E_β endpoint in the observed spectrum, which is discussed later in this chapter. Indeed, the discrepancy disappears if the tkeV values are corrected for resolution broadening, as shown in Figure 2c. The overall trend of these data readily illustrates the influence of a probability like that in Figure 1.

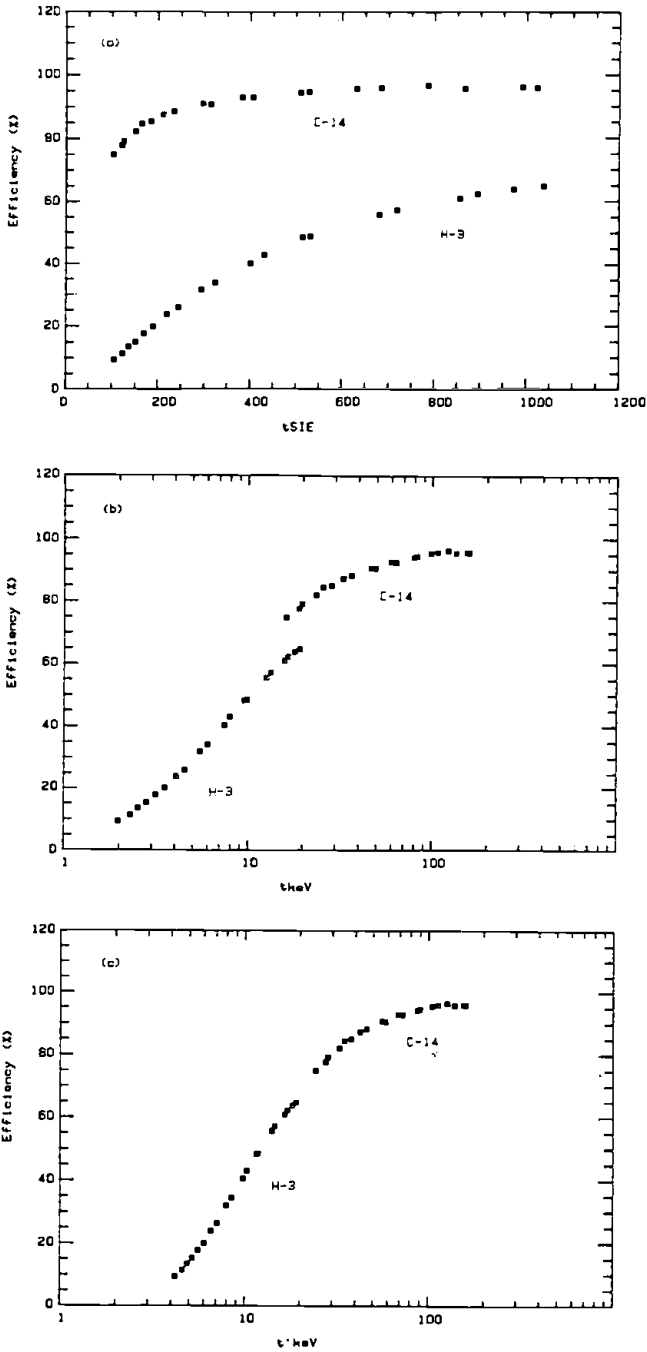


Figure 2. Typical efficiency data for TRI-CARB 2000 CA liquid scintillation analyzer: (a) efficiency vs $tSIE$ quench parameter, (b) efficiency vs $t'keV \equiv tSIE/1000 \times E_{\beta}$ and (c) efficiency vs $t''keV = t'keV$ corrected for resolution broadening.

Mathematical Basis

A perfectly ideal liquid scintillation detector would count a sample spectrum $R(E)$ with 100% efficiency, and its energy scale would correspond to the total photons produced per decay event. Integrating $R(E)$ over its range yields the sample decay rate, r_d . The detected sample spectrum $S(E')$ does not have 100% efficiency, and its energy scale corresponds only to different fractions of the total photons per event. Thus, integration of $S(E')$ over its range yields an observed count rate, r_c , that is less than, r_d . These two rates define the sample counting efficiency as

$$\epsilon = \frac{r_c}{r_d} = \frac{\int S(E') dE'}{\int R(E) dE} \tag{1}$$

Here, as in all subsequent discussion, the energy integrals are over their respective spectral ranges (0 to max) for the sample.

The present approach explores the relation between the observed $S(E')$ and the ideal $R(E)$ spectra, so that ϵ may be determined without using known standards. Proper usage of standards can be cumbersome for samples containing multiple α , β , τ , ce, X-ray, and/or EC/Auger emitting radionuclides. The 100% detection $R(E)$ spectrum is transformed to $S(E')$ by the scintillation detection processes, viz

$$\begin{aligned} S(E') dE' &= \int R(E) dE p(E'|E) dE \\ S(E') &= \int R(E) p(E'|E) dE \end{aligned} \tag{2}$$

where $p(E'|E) dE'$ is the probability that E total photons per decay yield E' detected photons in the range dE' . Assuming that an inverse transform exists for Equation 2, $R(E)$ is solved as

$$R(E) = \int S(E') f(E|E') dE' \tag{3}$$

where $f(E|E')$ is the inverse transformation kernel. Equations 2 and 3 require that

$$\begin{aligned} R(E) &= \int [\int R(E^*) p(E'|E^*) dE^*] f(E|E') dE' \\ &= \int R(E^*) [\int p(E'|E^*) f(E|E') dE'] dE^* \\ &= \int R(E^*) \delta(E^* - E) dE^* \\ &= R(E) \end{aligned} \tag{4}$$

where $\delta(E^* - E)$ is the Dirac delta function, and E^* is a dummy integration variable. This delta function defines $f(E|E')$ in relation to $p(E'|E^*)$ as

$$\int p(E'|E^*) f(E|E') dE' = \delta(E^* - E) \tag{5}$$

Equation 5 is obtained directly from Equation 4, and solving it for $f(E|E')$ requires that $p(E'|E^*)$ be defined. A useful example is

$$\begin{aligned} p(E^l|E^*) &= \delta(E^l/c - E^*) p(E^*) \\ f(E^l|E^l) &= \delta(cE - E^l) f(E^l) \end{aligned} \quad (6)$$

whereby each E^l of $S(E^l)$ corresponds to a single E or $R(E)$, and vice versa, per $E^l = cE$. To illustrate that the Equation 6 relations constitute a solution of Equation 5, they are substituted directly into Equations 2 and 3, to yield

$$\begin{aligned} S(E) &= \int R(E^*) \delta(E^l/c - E^*) p(E^*) dE^* = p(E^l/c) R(E^l/c) \\ R(E) &= \int S(E^l) \delta(cE - E^l) f(E^l) dE^l = f(cE) S(cE) \end{aligned} \quad (7)$$

Substituting $E^l = cE$ in the above expressions and then multiplying yields the relationship between $p(E)$ and $f(E)$. The specific relations are

$$\begin{aligned} S(cE) R(E) &= p(E) R(E) f(cE) S(cE) \\ p(E) f(cE) &= 1 \text{ or } p(E) = 1 / f(cE) \end{aligned} \quad (8)$$

Using Equations 6 and 8 in Equation 5 yields

$$\begin{aligned} \int p(E^l|E^*) f(E^l|E^l) dE^l &= \int \delta(E^l/c - E^*) p(E^*) \delta(cE - E^l) f(E^l) dE^l \\ &= \delta(E - E^*) p(E^*) f(cE) \\ &= \delta(E - E^*) p(E) f(cE) \\ &= \delta(E - E^*) \end{aligned} \quad (9)$$

which completes the proof. The above example is somewhat ideal, because any number of coincident photons (E^l), which is less than the emitted total (E), may be detected. Yet, for sufficiently narrow distributions of E^l , the δ -function approximation with $E^l = cE$ can be reasonable. This approximation is tested in the present study, where the $R(E)$ and $S(E^l)$ are related by $p(E)$ per Equations 7 and 8.

Model Approximation

The number of photons produced per scintillation event ultimately defines the detection efficiency for the event. The TRI-CARB 2000 CA/LL spectra are calibrated so that about 10 photons are produced for each keV for unquenched β -emissions.¹⁵ For α emissions, photon production per keV is lower by an order of magnitude;¹⁵ however, their monoenergetic α -energies are well above 4000 keV, producing numerous photons and efficiencies of almost 100%. For quenched samples, the photon production is lower, as reflected by their contracted spectra.

The two PM tubes detect only a fraction of the photons that are emitted in an event. These PM tubes detect the photons with probability p^1 and p^2 , and the probability for non-detection is p_0 . For N emitted photons, the trinomial

distribution gives the probability for detecting n_1 and n_2 photons on the PM tubes and missing detection of $n_0 = N - n_1 - n_2$. This trinomial distribution is described by

$$P(n_0, n_1, n_2|N) = \frac{N!}{n_0! n_1! n_2!} p_0^{n_0} p_1^{n_1} p_2^{n_2}$$

$$\text{all} \sum P(n_0, n_1, n_2|N) = (p_0 + p_1 + p_2)^N = 1 \tag{10}$$

where the summation “all” refers to all possible n_0, n_1, n_2 combinations. Suppose that at least n coincidences for the PM tubes are required for event detection. The probability for detecting n or more coincidences is

$$P(\geq n|N) = \sum_{\geq n} P(n_0, n_1, n_2|N) \tag{11}$$

where the “ $\geq n$ ” means that both n_1 and n_2 are at least as large as n for terms included in the summation. The $P(\geq n|N)$ is essentially the same as the $p(E^l|E)$ discussed in the preceding section, where E is proportional to N emitted photons and E^l represents the distribution of detected photons governed by the $\geq n$ range. With the δ -function approximation $P(\geq n|N)$ becomes $p(E)$. Equations 10 and 11 were used to generate the $P(\geq n|N) = p(E)$ plotted in Figure 3, and these illustrate that the detection probability is very low for small N and monotonically increases toward an asymptotic value of 1. An energy scale based on 10 photons per keV is added for reference to E ; the corresponding average E^l would be expected to be $(p_1 + p_2) \times E$; however, the energy scale of the TRI-CARB 2000 CA/LL is calibrated so that $c = 1$, yielding $E^l = E$. Thus, the $p(E)$ and $p(E)$ are identical in the present study.

It should be emphasized that the above $p(E)$ models all use the δ -function approximation that was discussed in the preceding section. Such models are reasonable for these preliminary tests, and should act as a guide to future improvements with more refined models. In fact, a good case can be made for the present trinomial distribution as a model by examining the distribution of the $(n_1 + n_2)$ detected photons, which represents the E^l distribution. The average $\langle n_1 + n_2 \rangle$ and its variance σ^2 are calculated using a binomial representation of the trinomial distribution, which is described as

$$1 = (p_0 + p_1 + p_2)^N = \sum_{\text{all}} \frac{N!}{(n_1 + n_2)! n_0!} (p_1 + p_2)^{n_1 + n_2} p_0^{n_0}$$

$$\langle n_1 + n_2 \rangle = (p_1 + p_2) N \tag{12}$$

$$\sigma^2 = (p_1 + p_2) (p_0) N = \langle n_1 + n_2 \rangle p_0$$

A more accurate estimate would sum over “ $\geq n$ ” as opposed to “all”; however, the above approximation is sufficient for the present study. Because $n_1 + n_2$ is proportional to E^l and N is proportional to E , these relations imply that $c =$

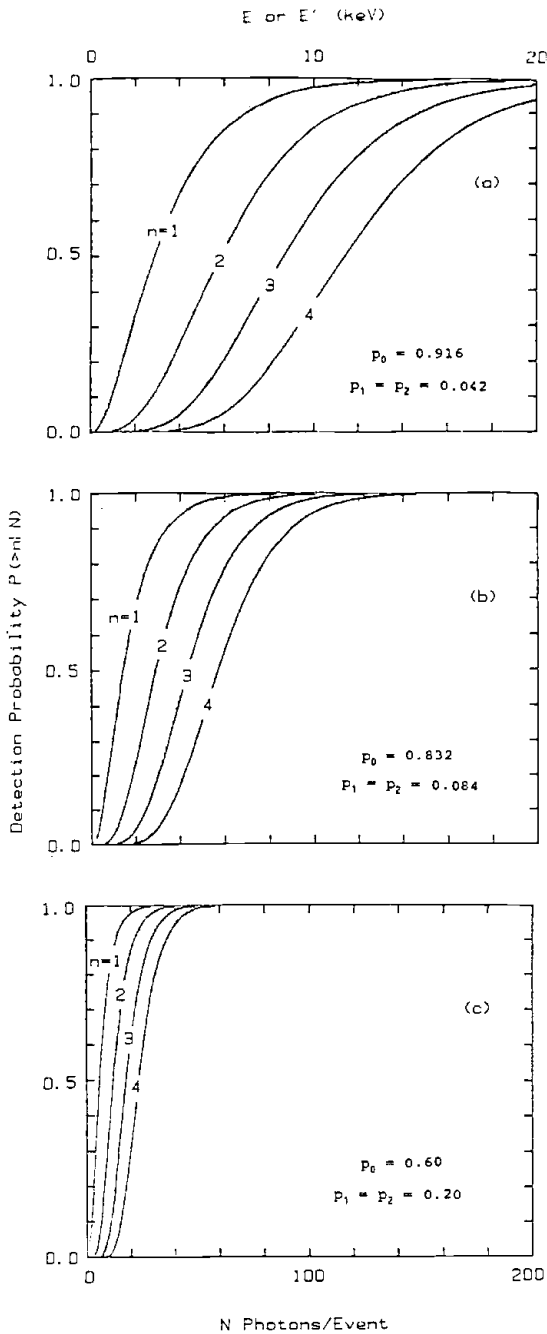


Figure 3. Detection probability $p(\geq n|N)$ vs photons/event N , for threshold detection of n coincident photons. The present study appraised the $p(\geq 1|N)$ of Figures a and b, and the $p(\geq 2|N)$ of Figure c.

$E^l/E = \langle n_1 + n_2 \rangle / N = p_1 + p_2$; however, as mentioned earlier, the TRI-CARB 2000 CA/LL is calibrated so that $c = 1$. Accordingly, Figure 3 includes scaled horizontal axes N , E , and E^l . Because the σ fluctuations about $\langle n_1 + n_2 \rangle$ are proportional to $N^{1/2}$, their range is narrowest for the lowest E^l , where the inverse transformation factor $f(E^l) = 1/p(E)$ is largest. For larger E^l , its broader range is not as crucial, because the transformation factor is relatively constant with a value near 1.

MEASUREMENTS

Two types of measurements were performed. The first used conversion electrons and Auger electrons of ^{57}Co to help identify reasonable $p(E)$ from calculations as shown in Figure 3. The second series of measurements accumulated ^3H and ^{14}C scintillation spectra to test the $p(E)$ for correcting the total count rate of the observed spectrum, $S(E)$, to the total decay rate of the real spectrum, $R(E)$.

A nominal $1.5 \mu\text{Ci/mL}$ ^{57}Co aqueous solution, dissolved as CoCl_2 , was provided by Isotopes Products Laboratories. A set of 20 quenched standards was prepared from this solution, in which 0, 50, . . . , and 950 μL of acetone were added to base cocktails, each composed of 18 mL of Optifluor, 2 mL distilled water, and 50 μL of the ^{57}Co solution. Standard 25 mL polyethylene counting vials were used. The TRI-CARB 2000CA/LL counted each sample for 10 min and stored its spectrum on floppy disk. The disk spectra were transformed for display analysis on an IBM/XT computer programmed with an EG&G Ortec ADCAM multichannel emulator. Representative spectra are shown in Figure 4.

Measurements for ^3H and ^{14}C were performed similarly. Some of the solutions were commercial standards from Packard Instrument Company; these were both quenched and unquenched and contained in nominal 25 mL glass vials. Other samples were prepared on site and used the 25 mL polyethylene vials. In particular, 500 μL of an NBS standard solution (NBS SRM-4927) with 33,720 dpm tritium was added to 2 mL of distilled water and 18 mL Optifluor for a base cocktail. Ten of these base solutions were counted, and then they were quenched by adding 50, 100, . . . , and 500 μL of acetone and recounted. Following this 500 μL of acetone was added to each of these samples to yield a set quenched with 550, 600, . . . , and 1000 μL of acetone. The spectrum for each sample was counted for 10 min and stored on floppy disk.

RESULTS

Selection of $p(E)$ from ^{57}Co Studies

The three spectra of Figure 4 illustrate how quenching contracts the observed spectrum $S(E^l)$ to lower energies. The Figure also illustrates the effect

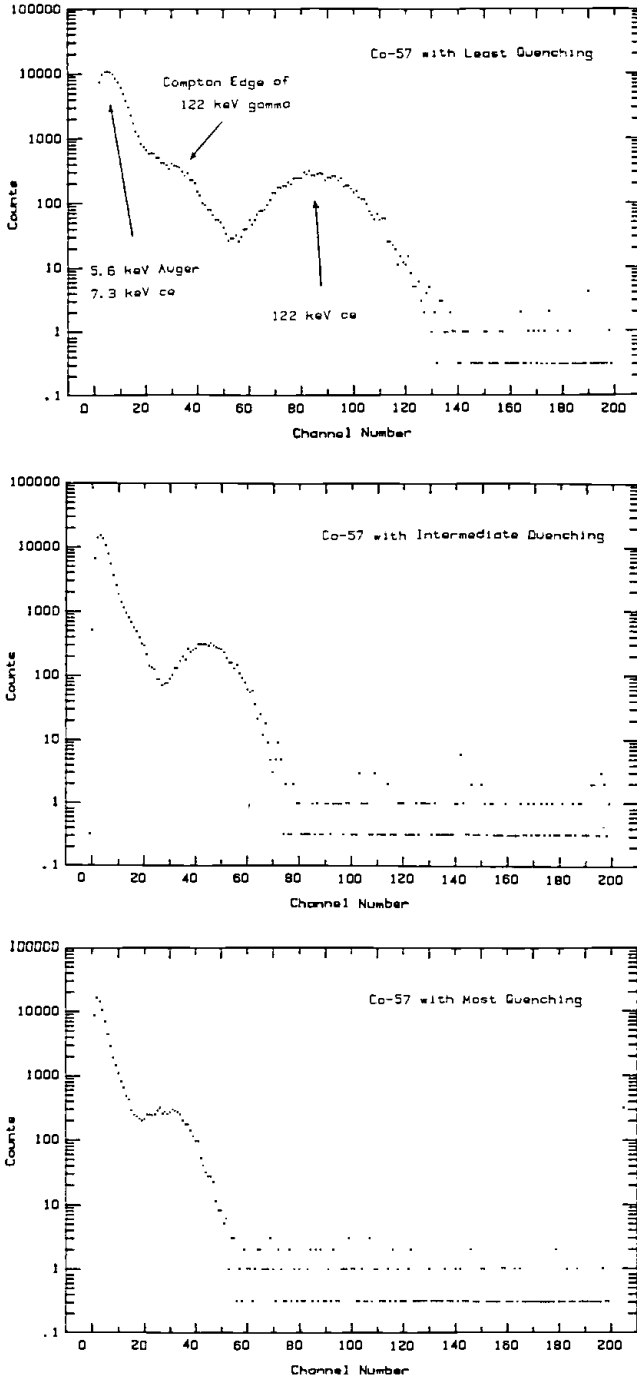


Figure 4. Liquid scintillation spectra of ^{57}Co with (a) least, (b) intermediate, and (c) most quenching. The dominant spectral components are identified.

of $p(E)$ on the lower end of these spectra. In particular, because $S(E) = p(E)R(E)$ per Equation 7, a larger fraction of the real spectrum $R(E)$ is eliminated from $S(E)$ as the spectra are contracted to lower energies.

Three peak regions appear in the spectra, which are all identifiable as ^{57}Co emissions.¹⁶ The highest peak includes K- and L-shell conversion electron (ce-K and ce-L) emissions of 115 and 122 keV associated with the 122 keV τ -ray and similar emissions of 129 and 136 keV associated with the 137 τ -ray. The 122 ce dominates this peak. A contribution for the photoelectrons produced by these gammas is also included in this highest energy peak. The lowest energy peak is due to ce- and τ -emissions associated with the 14.4 keV transition and also Auger and X-ray emissions associated with the EC decay. The 7.3 keV ce-K is the dominant emission for the 14.4 keV transition, and a comparably intense 5.6 keV Auger emission dominates the Auger/X-ray cases. Emissions contributing to the lower peak effectively range from 5.6 to 14.4 keV. (Other Auger emissions of less than 1 keV were either quenched beyond detection or detected per summing with the larger peaks). The middle peak region is not well pronounced and includes Compton electrons produced by the 122 and 136 keV gammas, corresponding to Compton edges of 39 and 47 keV. The Compton edge of the 122 keV gamma is dominant.

The ^{57}Co spectral data were used as a guide for selecting the $p(E)$. Analyses of the 20 quenched spectra yielded peak centroids and areas. Figure 5 plots the centroid ratio of the highest and lowest peaks against the centroid of the highest peak. The ratio is about 18 and constant, if the quenching does not move the highest peak below channel 55. As quenching contracts the peaks to

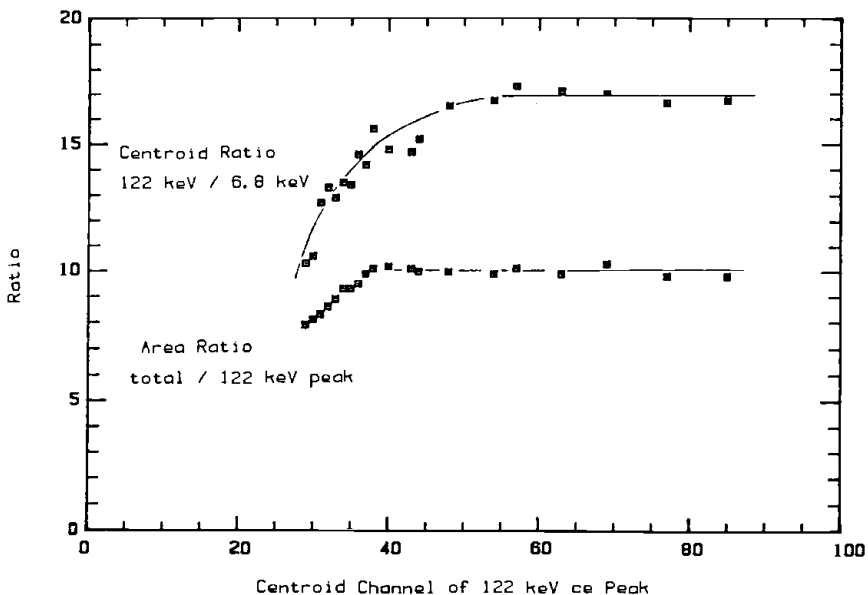


Figure 5. Centroid ratio and area ratio, measured for quenched ^{57}Co samples.

lower channels, the true centroid of the lowest peak is lost due to its low $p(E)$, and an artificially high centroid is determined. Because this drop in ratio begins as the highest peak falls below channel 55, the $p(E)$ begins to affect the lowest peak when it drops below channel $55/18 = 3.1$. The ratio of total spectral counts to highest peak area provides a less sensitive check, as Figure 5 illustrates. Its departure from constancy is just observable when the highest peak centroid drops below channel 40. Overall, these tests imply that the true departure is above channel 3. All trinomial predictions of Figure 3 were selected to be consistent with this condition.

As a further guide in selecting $p(E)$, the centroid and FWHM of the 122 keV peak in Figure 4a were examined in terms of Equation 12. Specifically, a $\langle n_1 + n_2 \rangle$ corresponding to centroid channel 85 and its σ of $\text{FWHM}/2.355 = 13.6$ yields

$$\langle n_1 + n_2 \rangle^2 / \sigma^2 = (p_1 + p_2) N / p_0 = (85/13.6)^2 = 39.1$$

Using the 10 photons/keV and 0.5 keV/channel calibration information,¹⁵ $N = 85 \times 10 \times 0.5 = 425$, and this yields $p_1 = p_2 = 0.042$ and $p_0 = 0.916$. These values are comparable to values used in efficiency models. Using a minimum of $n = 1$ photon coincidences, Equation 11 yields the $p(E)$ of Figure 3a for this case, which is identified as Model #1 $p(E)$.

The Model #1 $p(E)$ must have $E \geq 5$ keV (channel 10) before it begins to approach 1, and this is considerably higher than the $E \geq 1.5$ keV (channel 3) deduced from the ^{57}Co studies; thus, other models of $p(E)$ that lie between these extremes were also examined. Model #2 rises twice as fast as Model #1, whereby $E \geq 2.5$ keV as $p(E)$ begins to approach 1. Model #3 is a modification of Model #2, in which $p(E)$ is reduced for the lower E values, in an attempt to provide a better empirical model. Finally, Model #4 requires a minimum of $n = 2$ coincidences, and the p_0 and $p_1 = p_2$ are selected to yield a good empirical model. The $p(E)$ values of each model are given in Table 1.

Application of $p(E)$ to ^3H and ^{14}C Spectra

The $p(E)$ models given of Table 1 were applied to the collected ^3H and ^{14}C spectra. In particular the decay rates for these spectra were calculated as

$$r_d = \sum S(E)/p(E) \quad (13)$$

where the sum is over all channels of the spectrum. The results for each model are given in Figure 6, where the ratio of predicted/known r_d values are plotted against the known efficiency, ϵ . For higher ϵ the ratio is close to 1, indicating that model predictions agree well with known values; however, for lower ϵ , the agreement falls off. This reflects the fact that the $p(E)$ corrects a larger portion of the spectrum for lower-energy (and thus lower ϵ) cases, as implied by Table 1 and Equation 13. Model #1, which corresponds more closely to earlier effi-

Table 1. Models of $p(E)$

Channel #	E keV	p(E)			
		Nidek #1	Model #2	Model #3	Model #4
0	0.25	0.01	0.01	0.01	0.0039
1	0.75	0.07	0.16	0.10	0.200
2	1.25	0.16	0.38	0.30	0.555
3	1.75	0.27	0.56	0.50	0.797
4	2.25	0.38	0.70	0.70	0.920
5	2.75	0.48	0.81	0.81	0.964
6	3.25	0.56	0.88	0.88	0.983
7	3.75	0.63	0.915	0.915	0.992
8	4.25	0.70	0.94	0.94	1.000
9	4.75	0.76	0.958	0.958	
10	5.25	0.81	0.971	0.971	
11	5.75	0.85	0.983	0.983	
12	6.25	0.88	0.992	0.992	
13	6.75	0.90	1.000	1.000	
14	7.25	0.915			
15	7.75	0.93			
16	8.25	0.94			
17	8.75	0.95			
18	9.25	0.958			
19	9.75	0.965			
20	10.25	0.971			
21	10.75	0.977			
22	11.25	0.983			
23	11.75	0.988			
24	12.25	0.992			
25	12.75	0.996			
≥ 26	≥ 13.25	1.000			

Notes: Model #1: $p_1 = p_2 = 0.042m$, $p_0 = 0.916$, $n = 1$, Model #2: $p_1 = p_2 = 0.084$, $p_0 = 0.832$, $n = 1$, Model #3: Model #2 modified at lower channels, Model #4: $p_1 = p_2 = 0.20$, $p_0 = 0.60$, $n = 2$.

ciency models,^{4,9,12} yields worse agreement than the other models, which were developed from semiempirical considerations.

A bootstrap technique can extend the application to lower efficiencies. If the measured total spectral countrate, r_c , is divided by the predicted decay rate r_d , an experimental pseudo-efficiency, e^l , may be defined as r_c/r_d . If the ratios of predicted/known r_d are plotted against their e^l , the plots of Figure 7 result for each model, thus, any measurement of e^l yields a predicted/known correction ratio k , from which the true decay rate may be calculated as r_d/k and $n = E/E^l$, so that Figure 7 yields $E = nE^l$ per measurement of E^l .

DISCUSSION

Each $p(E)$ model is demonstrated to yield sample efficiencies to $\approx 10\%$ for efficiencies ranging from 0.1 to 1.0, provided that the bootstrap technique can be applied, as seen in Figure 7. No $p(E)$ was found to yield efficiencies that agreed with the known ones over the entire efficiency range tested, as shown in Figure 6. The δ -function model, for which the $p(E)$ models are based, appar-

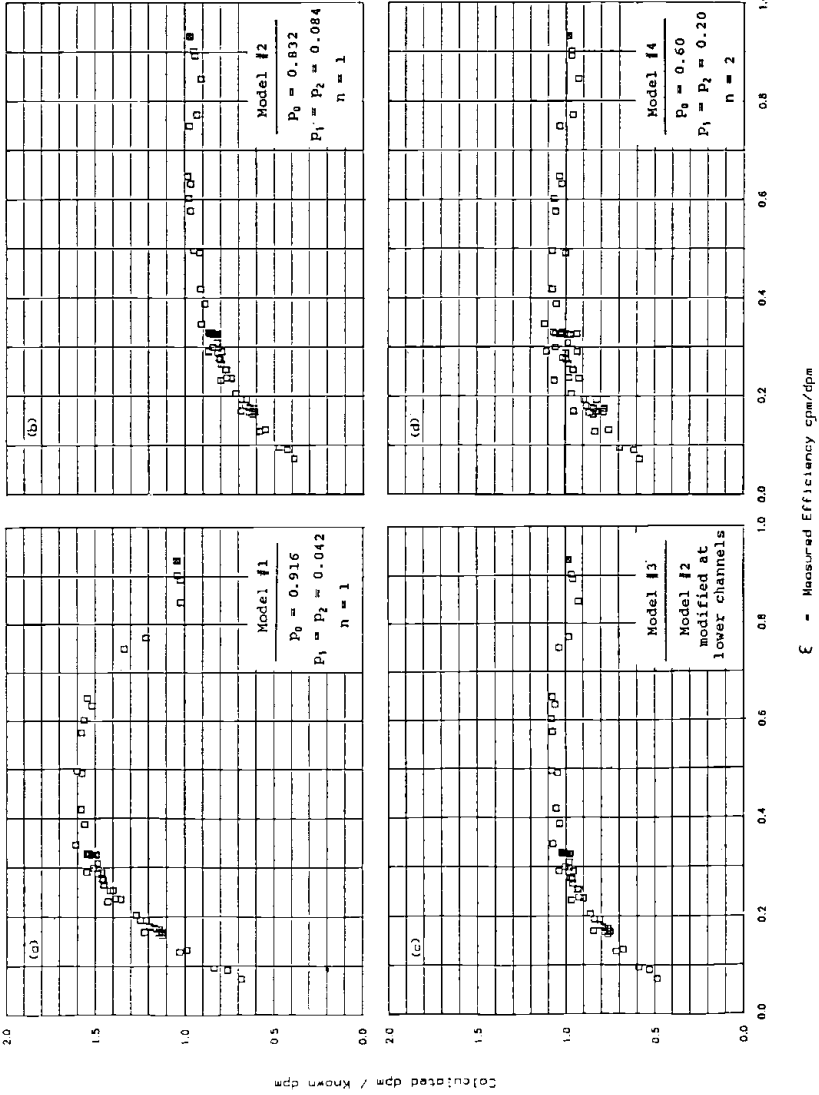


Figure 6. Comparison of predicted/known decay rates as function of efficiency ϵ , for the four models examined.

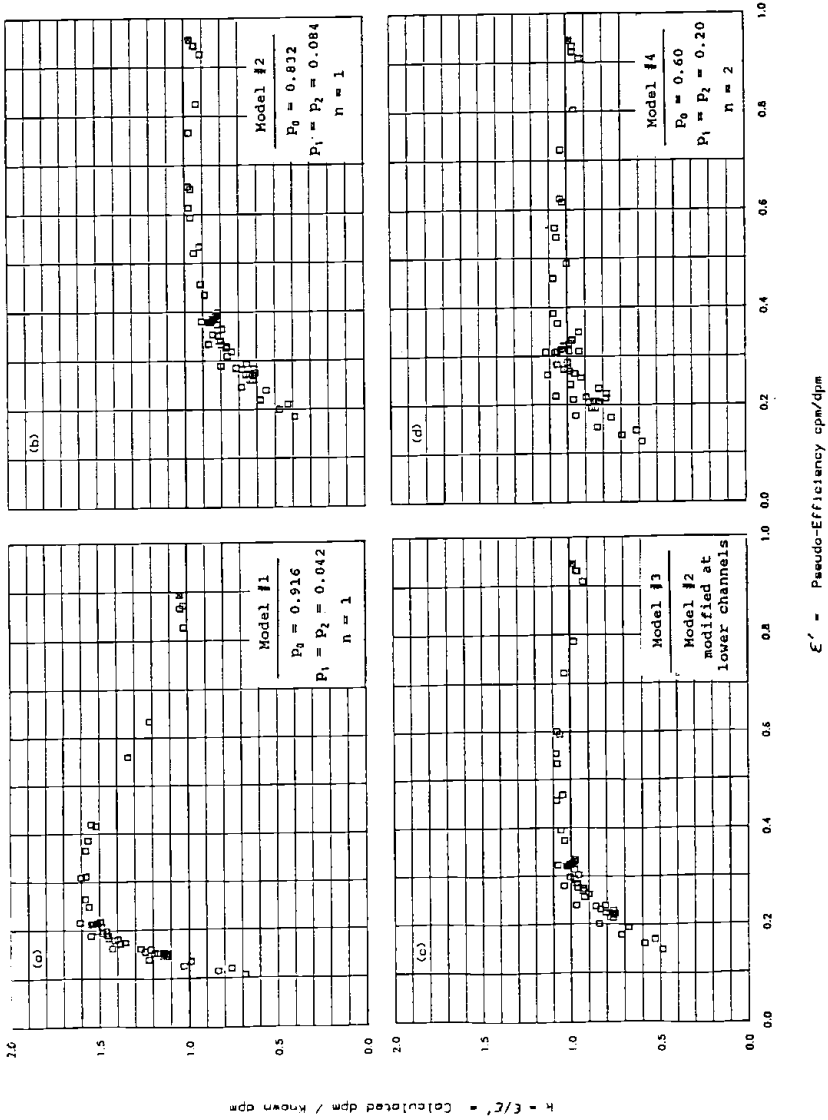


Figure 7. Comparison of predicted/known decay rates as function of pseudo-efficiency, ϵ' , for the four models examined.

ently breaks down for the lower efficiency cases. Improvement beyond the present treatment will require development of a more realistic inverse transformation kernel $f(E|E')$, to convolute the observed spectrum $S(E')$ to its ideal form $R(E)$.

Liquid waste samples complying with DOT regulations must be less than 2 nCi/g, or effectively 4440 dpm/mL. For a 3 mL sample and a 10 min counting time, a total of 133,200 decays would occur. For ϵ down to 0.1 (per measurement of ϵ), at least 13,000 counts should be observed, and most of these would be at the lower end of the spectrum so that the $p(E)$ -corrected counts would have reasonable counting errors. For higher ϵ , the counting errors will be even smaller; thus, the method should have application for certifying liquid waste for transport. Model #1, which yields overestimates as high as 60%, could be a useful conservative analysis method for this application.

Some liquid waste can fall outside the above range of application. For example, some liquids may require dilution so that a 3 mL scintillation sample would contain less effective activity than its original solution. Also, the sample may have quenching that renders an efficiency below 0.1. In these cases, the $p(E)$ for the upper channels would still be 1; however, a low energy standard such as tritium can be used to spike an identical sample to appraise the low energy portion of the spectrum.

For the β -components of the spectrum, the calibration of Figure 2c could be used upon proper identification of the endpoints $E_\beta^|$. The endpoints on the $E^|$ scale are distorted as $aE_\beta + bE_\beta^{1/2}$ or $N + bN^{1/2}$, according to resolution broadening predicted by Equation 12 and illustrated in Figure 4. Here aE_β is the true spectral endpoint; which appears higher by $bE_\beta^{1/2}$ due to resolution broadening. The factor $a = F(E)$ is the scintillation efficiency, which has a broad maximum at ≈ 200 keV.⁹ Using Figure 4; $b = 3.45$ keV^{1/2} was estimated from the ce peak. Because the $E^|$ scale is normalized to yield a good fit with the E_β endpoints, it is not strictly proportional to E_β , although the linear approximation is reasonably good. The results of Figure 2c assume that the unquenched ³H and ¹⁴C cases correspond to their endpoints of $E_\beta^| = 18.6$ and 156.5 keV, but their unquenched cases are given by

$$E_\beta^| = (tSIE/1000) e_\beta + b [(tSIE/1000) e_\beta]^{1/2} \quad (14)$$

where e_β is the effective aE_β pertaining to the normalized $E_\beta^|$ scale for the unquenched sample ($tSIE = 1000$). It is determined for ³H and ¹⁴C using their corresponding unquenched $E_\beta^|$. The $E_\beta^|$ of Figure 2c and Equation 14 are given in units of $t^|$ keV. It should be recalled that this method assumes that the β -spectra have the same relative profiles, but this is not always true. For example, ²⁴¹Pu with $E_\beta = 20.82$ keV has a lower efficiency than ³H with $E_\beta = 18.6$ keV,¹² this is contrary to the monotonic energy trend in Figure 2c. Here the profiles differ so much that the ²⁴¹Pu average β -energy of 5.23 keV is lower than that of 5.69 keV for ³H.¹⁷ Some care must be exercised in using this technique.

ACKNOWLEDGEMENTS

The author acknowledges useful discussions with K.J. Hofstetter, W.L. McDowell, and R.W. Taylor. The author also thanks C.D. Ouzts for conducting many of the laboratory measurements.

The information contained in this paper was developed under Contract No. DE-AC09-88SR18035 with the U.S. Department of Energy.

REFERENCES

1. Code of Federal Regulations, 49CFR173.403(g), June, 1986.
2. Ishikawa, H. and M. Takiue. *Nucl. Instr. and Methods*, 112:437-442 (1973).
3. Ishikawa, H., M. Takiue, and T. Aburai. *Int. J. Appl. Radiat. Isot.* 35:463-466 (1984).
4. Coursey, B.M., W.B. Mann, A. Grau Malonda, E. García-Toraño, J.M. Los Arcos, J.A.B. Gibson, and D. Reher. *Appl. Radiat. Isot.* 37:403-408 (1986).
5. Kobayashi, Y., M. Kessler, and S. van Cauter, *Amer. Lab.*, 20:160-167 (1988).
6. Houtermans, H., *Nucl. Instr. and Methods*, 112:121-130 (1973).
7. De Filippis, S.J. *Trans. Am. Nuc. Soc.* 50:15-16 (1985).
8. De Filippis, S.J. and S.C. van Cauter. *Trans. Am. Nuc. Soc.* 50: 22-23 (1985).
9. Broda, R., K. Pochwalski, and T. Radoszewski. *Appl. Radiat. Isot.* 39:159-164 (1988).
10. Pochwalski, K., R. Broda, and T. Radoszewski. *Appl. Radiat. Isot.* 39:165-172 (1988).
11. Grau Malonda, A. and B.M. Coursey. *Appl. Radiat. Isot.* 39:1191-1196 (1988).
12. Coursey, B.M., A. Grau Malonda, E. García-Toraño, and J.M. Los Arcos, *Trans. Am. Nuc. Soc.* 50:13-15 (1985).
13. Grau Malonda, A. and E. García-Toraño. *Int. J. Appl. Radiat. Isot.* 33:249-253 (1982).
14. Jordan, P. *Nucl. Instr. and Methods*, 97:107-111 (1971).
15. Model 2000CA TRI-CARB Liquid Scintillation Analyzer/ Operation Manual, Publication No. 169-3029, Packard Instrument Co, 1987.
16. *Radionuclide Transformations—Energy and Intensity of Emissions*, Annals of ICRP—Publication 38, 11-13 (1983).
17. Koehler, D.C. Radioactive Decay Data Tables, DOE/TIC-11026 (1985).

